International Atomic Energy Agency

INDC(CSR)-3/L

INDC INTERNATIONAL NUCLEAR DATA COMMITTEE

Neutron Cross Sections at 14 MeV

I. Ribansky and S. Gmuca

June 1982

IAEA NUCLEAR DATA SECTION, WAGRAMERSTRASSE 5, A-1400 VIENNA

Reproduced by the IAEA in Austria
June 1982
82-3595

INDC(CSR)-3/L

Neutron cross sections at 14 MeV

I. Ribanský and Š. Gmuca

Institute of Physics, Electro-Physical Research
Centre of the Slovak Academy of Sciences,
Dúbravská cesta, 842 28 Bratislava,
Czechoslovakia

Content

1. Neutron activation cross sections measurements at 14 MeV

The activation method is in principle very simple and the cost of all necessary equipments needed to perform the neutron activation measurements is not very high. These are the main reasons why many small laboratories - including the department of nuclear physics of our Institute - are actively using 14 MeV neutron generators for measurement of neutron activation cross sections (NACS). This type of experimental data are needed for the calculations of fusion reactors and still a large number of requests for fast neutron cross section data are listed in latest WRENDA [1]. There exist, however, large differences between experimental values of NACS measured at different laboratories [2]. It is therefore worthwhile to look carefully for possible sources of these discrepancies with the aim to improve the reliability of measured NACS and - - in this way - to increase their practical as well as physical significance.

Having this in mind we have started a systematic investigation of several methodological problems connected with the activation method. Some results we have obtained during last two years will be reviewed in the first section of this report.

1.1 Calibration of Ge(Li) detector in close geometry

One of the modern and in present time often used methods of determination of NACS is the Ge(Li) γ-spectroscopy of the reaction products. In order to achieve the smallest possible statistical error of the full energy peak (FEP) area

one has to measure the activated samples at the smallest distance from the Ge(Li) detector. This arrangement requires a rather precise knowledge of the absolute detection efficiencies - ε_{FEP} and ε_{TOT} - in order to calculate the coincidence summing corrections [3] and to eliminate one source of systematic errors.

We have determined ε_{FEP} and ε_{TOT} in close geometry (C) using the method of transformation curves [4].

The Ge(Li) detector was calibrated at far geometry (F) using the standard set of point γ-ray sources (^{241}Am, ^{57}Co, ^{203}Hg, ^{133}Ba, ^{137}Cs, ^{60}Co and ^{88}Y). The distance sample - to - detector was 17 cm in order to make the coincidence summing corrections negligible for multi-line sources. The activity of our sources was known with the accuracy 1% (at 3σ confidence level). Using the χ^2-criterion the experimental points of $\varepsilon_{FEP,F}$ were fitted by the the following function

$$\varepsilon_{FEP,F}(E_\gamma) = a_1 T \exp(-a_2\mu)(1-\exp(-a_3\mu))/\mu \times \\ \times (\tau + a_4(\sigma+\kappa)\exp(-a_5 \ln E_\gamma - a_6 \ln^2 E_\gamma)), \qquad (1)$$

where T describes the absorption in the detector's cover; μ, τ, σ and κ are attenuation coefficients for the total absorption, photo-effect, Compton effect and pair production. The function (1) is close to 5 - parametric function of Hnatowicz [5]. The uncertainty of $\varepsilon_{FEP,F}$ evaluated using covariance matrix of parameters was less than 1% (1σ) in the energy interval 60-2000 keV.

The transformation curve from F to C geometry was constructed by means of "single-line" noncalibrated sources (^{241}Am, ^{109}Cd,

^{57}Co, ^{203}Hg, ^{85}Sr, ^{137}Cs, ^{54}Mn and ^{65}Zn). Their geometrical shape (disc ø 16 mm) was identical with samples used for the neutron activation. For determination of $\varepsilon_{FEP,C}$ at higher energies we used ^{88}Y (1836 keV) measured by the coincidence method [4]. The experimental points of the transformation curve were then fitted by the function

$$R(E_\gamma) = a_1 \exp(-a_2\mu)(1-\exp(-a_3\mu))/(1-\exp(-a_4\mu)) \times \times \exp(-a_5 \ln E_\gamma - \ln^2 E_\gamma) \qquad (2)$$

which is in fact the ratio of two functions of the type (1). The uncertainty of $R(E_\gamma)$ was less than 1% (1σ) in the whole E_γ interval. The $\varepsilon_{FEP,C}$ is then given by

$$\varepsilon_{FEP,C}(E_\gamma) = R(E_\gamma)\,\varepsilon_{FEP,F}(E_\gamma). \qquad (3)$$

The uncertainty of $\varepsilon_{FEP,C}$ was less than 1.5% (1σ).

The total detection efficiency ε_{TOT} in C-geometry was determined essentially in the same way as ε_{FEP}. The only difference was that ^{57}Co and ^{60}Co were treated as "single-line" sources emitting γ's with the mean energy of 124 keV and 1253 keV respectively. The experimental points were fitted by the function

$$\varepsilon_{TOT,F}(E_\gamma) = a_1 T \exp(-a_2\mu)(1-\exp(-a_3\mu)) \qquad (4)$$

and the transformation curve by the function (2). The uncertainty of $\varepsilon_{TOT,C}$ was less than 5% (1σ) which is sufficient to keep the error due to coincidence summing corrections below 2%.

The efficiencies ε_{FEP} and ε_{TOT} are displayed in fig.1

and the transformation curves in figs. 2 and 3.

1.2 Analysis of complex γ-ray spectra

The primary quantity which is needed for determination of NACS when Ge(Li) γ-spectroscopy is used is the FEP area. The FEP of interest often appears in close proximity of other FEP's or is a part of a multiplet and it is therefore necessary to process γ-ray spectra with the help of a computer. Several sophisticated codes were worked out for that purpose (e.g. SAMPO, HYPERMET). To run those codes a relatively large computer is needed. With respect to our computing possibilities we have worked out the code GWENN (see ref. [6] and references there-in) especially for our mini-computer TPA-70 (28K core memory + disc). GWENN capabilities are comparable with those of the above-mentioned codes. Next, GWENN can be further reduced to fit computers with still smaller memory.

GWENN is divided in three parts (INITAL, SEARCH and FIT) which can create overlaying segments in smaller computers. Subroutine INITAL reads input data and analyzes control commands. Subroutine SEARCH identifies peaks in a specified region and prepares initial values of peak parameters needed for nonlinear least square fit (subroutine FIT). The solution of this task is based on an analytical method utilizing smoothed second differences for peak identification, nonitera-tive method for the fit of a peak by the Gaussian and striping procedure for decomposition of multiplets. Subroutine FIT fits the specified portion of a spectrum by the nonlinear least square method.

In the region of FEP the response function of Ge(Li) detector is represented by a slightly modified semiempirical function proposed by Phillips and Marlow [7]

$$F(i) = G(i) + D(i) + S(i) + B(i) \qquad (5)$$

where i is the channel number, G is the Gaussian, D represents the exponential low energy tail of FEP, S describes the amplitude difference between the left and the right side of FEP and B is the background approximated by a polynomial of the second order. For m peaks the function (5) has 2m+6 free parameters.

The parameters of (5) are estimated by minimalization of the weighted normalized least square functional Q^2. This is performed by the Gauss - Newton method with linearization of (5). This method facilitates sufficiently rapid convergence of the iteration process (typically 3-4 iterations are needed). The magnitude of the iteration step is optional. The iteration process is stopped if (i) the norm of the Q^2 gradient or (ii) the relative change of Q^2 after two successive iterations or (iii) the value of Q^2 drops below the value selected.

GWENN is written in a modular form. This enables to create simpler versions of GWENN according to the user requirements. For example INITAL + SEARCH represents a code for fast automatic analysis with noniterative fit; the combination INITAL + +FIT analyzes the choosen part of a spectrum by a nonlinear least square method using the function (5). In the last case the initial values of parameters are given manually. Up to ten peaks can be fitted simultaneously and the region lenght is li-

mited only by the accessible memory. The output of diagnostic information is sufficiently complex and its amount selectable. GWENN was tested under many different conditions and is in a routine use now. In fig. 4 a fitted part of Eu γ-ray spectra is displayed.

1.3 Automatization of activation measurements

In an effort to increase the efficiency and the reliability of activation measurements and to remove another source of systematic errors we have automatized the measuring process to the maximum possible extent with respect to the possibilities of our laboratory.

The automatization of measurement is performed with the help of our mini-computer TPA-70 which controls the whole experiment. All instruments and facilities used in the experiment are connected to the computer via the CAMAC system [8]. Block scheme of the experiment for activation measurements is in fig. 5.

The control program is written in FORTRAN. It enables to plan the whole measuring process, performes acquisition and storage of data, records all changes due to external interferences of the experimentator, performs communication with the operator of the neutron generator (our NG is not adapted for control by a computer) and prepares the complete report about the experiment after the end of measurement.

The neutron yield is measured by two scintillation detectors: the first detector, PR, measures the energy of recoiled protons and the other one, Li, detects thermalized neutrons by the lithium - glass scintillator (fig. 5). The PR-detector starts the measurements. The time variation of neutron yield is expli-

citely taken into account in calculations of NACS. Both neutron detectors are calibrated before each run with the help of $^{27}Al(n,p)$ and $^{56}Fe(n,p)$ reactions.

All time intervals are measured by the central clock generator which also controls the counters of neutron detectors. Signals from Ge(Li) detectors are processed by ND 4420 MCA. Each γ-spectrum is immediately transfered through CAMAC and stored on the disc in order to make MCA free for next measurement. In this way we can obtain maximum amount of information about the reaction studied and possibly other reactions whose products can be identified in γ-spectra. Gamma spectra are processed off-line with the help of GWENN code [6].

1.4 Neutron activation cross sections on Nd isotopes

Using the Ge(Li) γ-spectroscopy we have measured NACS on Nd isotopes [8]. The motivation for this work was that several NACS are not known and the published results show large discrepancies. The last fact represents a persistent problem [2] which lowers the practical and the physical significance of neutron activation measurements at 14 MeV. Our aim was to eliminate at least several sources of systematic errors and to identify possible causes of differences in the published results. We have used besides the natural samples also enriched samples in order to suppress the influence of the interference reactions; we have carefully applied corrections for coincidence summing and selfabsorption of low energy gammas in the sample; for the determination of NACS we have used all well identified γ-lines belonging to a given product in order to choose the most consistent set of γ-intensities for cal-

culation of NACS. Next we have taken explicitely into account the time variation of the neutron yield in order to eliminate systematic errors due to the nonequality of halflives of monitoring and measured reactions resp.

The cross sections were calculated according to the relation

$$\sigma_g = \sigma_m \frac{\lambda_m I_T}{\lambda_g - \lambda_m} + \frac{e^{\lambda_g (T_0+T_V)}}{\left[1-e^{-\lambda_g T_M}\right] \int_0^{T_0} e^{\lambda_g t} \phi(t) dt} \left\{ k \frac{P_\gamma A}{\varepsilon_\gamma I_\gamma \eta G} - \frac{\sigma_m \lambda_m I_T}{\lambda_g - \lambda_m} \times \right. \tag{6}$$

$$\left. \times e^{-\lambda_m (T_0+T_V)} \left[1-e^{-\lambda_m T_M}\right] \int_0^{T_0} e^{\lambda_m t} \phi(t) dt \right\}$$

where σ_m, σ_g, λ_m, λ_g are cross sections and decay constants of the isomeric and the ground state resp.; T_0, T_V, T_M are the irradiation, cooling and measurement times; I_T, I_γ are the absolute γ-transition intensities of the isomeric and the ground state resp.; ε_γ, P_γ are the absolute FEP detection efficiency and FEP area; A, η, G is the atomic weight, the isotopic abundance and the weight of the sample; ϕ is the relative neutron flux and k is the calibration coefficient of the neutron monitor. Eq. (6) can easily be reduced for simpler cases: (i) if there is no m-state we put $I_T=0$, (ii) if we measure only σ_m we put $I_T=0$, g=m and the subscript γ then refers to the m-state. We note that eq. (6) implies that $\sigma_{tot} = \sigma_m + \sigma_g$ can be measured only if $\lambda_m \gg \lambda_g$, $I_T \approx 1$ and the second term in curly brackets is close to zero.

During the processing of experimental data we have found that our values of NACS are mostly influenced by I_γ's. These

were taken from refs. [9, 10, 11]. The basic feature of those data was their mutual inconsistency. Further, in cases we succeeded to determine the FEP areas with sufficient accuracy for several γ-transitions belonging to a given reaction product, the values of corresponding NACS differed often by several tens of per cents for a given set of I_γ. In these cases the NACS were calculated as a weighted average using I_γ's for which the mutual deviations of the corresponding NACS were the smallest. We have recalculated - whenever it was possible - the results of other authors with γ-intensities we have used. We have found that in great majority of cases the difference of our results and those recalculated was several tens of per cents which grossly exceeds the experimental errors quoted.

The details of our measurements and the comparison of our results with those of other authors are given in [8]. In tab. 1, 2 and 3 we report the adopted values of NACS for Nd (n,x), x = 2n,p,α reactions. We note that the NACS for ^{142}Nd(n,p) ^{142}Pr and ^{144}Nd(n,p)^{144m,g}Pr were measured for the first time.

Tab. 1 Details of (n,2n) cross section measurements and adopted cross sections

Reaction	Reaction product decay data			Adopted cross section
	$T_{1/2}$	E_γ (keV)	I_γ	(mb)
$^{142}Nd(n,2n)^{141m}Nd$	62.4s	756.5	0.915	756 ± 70
$^{142}Nd(n,2n)^{141g}Nd$	2.49h	145.4	0.0022 [a]	
		1126.9	0.0075 [a]	778 ± 73
		1292.6	0.0012 [a]	
				$1544 \pm 101^{+}$
$^{148}Nd(n,2n)^{147}Nd$	11.1d	319.4	0.0205 [b]	
		531.0	0.133 [b]	1780 ± 50
$^{150}Nd(n,2n)^{149}Nd$	1.73h	114.3	0.16 [c]	
		211.3	0.23 [c]	1703 ± 82
		654.8	0.084 [c]	

a) Ref. [10], b) Ref. [11], c) Ref. [9]

+ $(\sigma_m + \sigma_g)$

Tab. 2 Details of (n,p) cross section measurements and adopted cross sections

Reaction	Reaction product decay data			Adopted cross section
	$T_{1/2}$	E_γ(keV)	I_γ	(mb)
$^{142}Nd(n,p)^{142}Pr$	19.1h	1575.7	0.037 [b]	13.8±1.1 [+]
$^{144}Nd(n,p)^{144m}Pr$	7.2m			1.7±0.6 [d]
$^{144}Nd(n,p)^{144g}Pr$	17.3m	696.5	0.0148 [b]	10.5±2.3 [d]
$^{145}Nd(n,p)^{145}Pr$	5.98h	675.8	0.0045 [c]	7.5±1.6
		748.3	0.0047 [c]	
$^{146}Nd(n,p)^{146}Pr$	24.1m	453.8	0.55 [c]	4.7±0.5
		735.7	0.089 [c]	
$^{148}Nd(n,p)^{148}Pr$	2.28m	301.7	0.91 [b]	2.14±0.17

b) Ref. [10], c) Ref. [9], d) determined from the decay curve of the ground state

[+] $(\sigma_m + \sigma_g)$

Tab. 3 Details of (n,α) cross section measurements and adopted cross sections

Reaction	Reaction product decay data			Adopted cross section (mb)
	$T_{1/2}$	E_γ(keV)	I_γ	
$^{142}Nd(n,\alpha)^{139}Ce$	137.5d	165.8	0.789	$6 \pm 0.9^+$
$^{144}Nd(n,\alpha)^{141}Ce$	32.5d	145.4	0.484	4.5 ± 0.6
$^{146}Nd(n,\alpha)^{143}Ce$	33.0h	293.3	0.514	4.2 ± 0.7
$^{148}Nd(n,\alpha)^{145}Ce$	3.0m	724.3	0.69	2.4 ± 0.2

$^+(\sigma_m + \sigma_g)$, I_γ from Ref. [11]

1.5 Theoretical analysis of 14 MeV neutron cross section data

It is well known, that the preequilibrium decay of composite nuclei originating in nuclear reactions induced by fast neutrons ($E_n \sim 14$ MeV) is not negligible. In (n,p) reactions on heavier nuclei this mode of decay is even dominant [12,13]. The Exciton model (EM) of nuclear reactions proposed by Griffin [14] is one of the phenomenological models which are capable to describe the angle - integrated high energy part of spectra of emitted nucleons. The quantum-mechanical foundation - though not without dispute - was given in [15,16].

Recently we have started systematic studies of EM in an effort to describe simultaneously the hard part of nucleon energy distribution from (n,x) reactions at ~14 MeV i.e. above the second nucleon threshold. The aim is to parametrize EM and try to describe the emission of complex particles. This problem seems to be still open [17]. The part of this program is to calculate NACS (specifically σ_{np}) at 14 MeV.

In our previous calculations [18] we tried to describe the neutron spectra above the threshold of the emission of the second neutron. This analysis has shown that the role of the target nucleus surface and presumably its shell structure is important for the reaction process. In our recent work we have used a modified EM which we shall briefly describe here. The energy distribution of emitted nucleons in (ν,x) reaction and in one component closed form formulation of EM is given by

$$\frac{d\sigma}{d\varepsilon_x} = \sigma_R(\varepsilon_\nu) \sum_{m_0=3} \frac{a_x(m)\, w_x(m,\varepsilon_x)}{\lambda_+(m,E) + \sum_{i=\nu,\pi} a_x(m) \int w_i\, d\varepsilon_i} D(m) \,, \qquad (7)$$

where $w_x(n, \varepsilon_x)$ is the nucleon emission rate with the energy ε_x from the state with n excitons, D(n) is the probability to find the composite nucleus in n state, λ_+ is the intranuclear transition rate to the more complex states, $a_x(n)$ is the probability that the excited particles will be of the type x, $\sigma_R(\varepsilon_\nu)$ is the optical model reaction cross section and E is the excitation energy.

The relations for w, λ_+ and D are given e.g. in [13]. We shall concentrate our discussion to those parameters which differ in our model from the usual EM.

The state density we have used is given by [19]

$$\omega_{p,h}(E) = \frac{g^n}{p!h!(n-1)!} \sum_{l=0}^{h} \binom{h}{l} (-)^l \left[E - lE_F\right]^{n-1} \Theta(E - lE_F), \qquad (8)$$

where g = A/13 is the single particle state density, n = p+h and Θ is the Heaviside function and E_F is the Fermi energy. In our model we have replaced E_F by E_H which we have interpreted as a depth of hole excitation [18]. Next we assume that only nucleons filling the last subshells of the target nucleus take part in the preequilibrium phase of the reaction. This assumption directly influences the calculation of $a_x(n)$.

In general (if we consider only nucleons)

$$a_x(m) = \frac{1}{p} N_x \;;\; x = \pi, \nu \qquad (9)$$

and

$$p = N_\pi + N_\nu \,,$$

where p is the number of excited particles and N_x is the number of excited particles of the type x. For the state (p,h)=(2,1) and the reaction ν + target nucleus we have

$$N_\nu = 1\frac{\sigma_{\nu\pi} n_\pi}{\sigma_{\nu\pi} n_\pi + \sigma_{\nu\nu} n_\nu} + 2\frac{\sigma_{\nu\nu} n_\nu}{\sigma_{\nu\pi} n_\pi + \sigma_{\nu\nu} n_\nu} = \frac{\alpha n_\pi + 2n_\nu}{\alpha n_\pi + n_\nu}, \qquad (10)$$

where n_ν , n_π are the number of nucleons in the subshells considered and α is the ratio of "free" nucleon-nucleon cross sections: $\alpha = \sigma_{\nu\pi}/\sigma_{\nu\nu} = \sigma_{\nu\bar{\pi}}/\sigma_{\pi\bar{\pi}}$. In eq. (10) the first term represents the probability to form the state with one excited proton and neutron and the second term the probability to form the state with two excited neutrons.

To test our model we have chosen "monoisotopic" target nuclei ^{51}V, ^{55}Mn, ^{56}Fe, ^{59}Co and ^{93}Nb in order to make the analysis simpler. Next these nuclei have a relatively large gap ($\sim$4 MeV) between last subshells [20] (except for protons in ^{93}Nb nucleus - see fig. 12) and the competition of α -emission is sufficiently weak.

The neutron spectra were taken from [21] and the proton spectra from [22]. In our calculations we have approximated the inverse cross sections by σ_R taken from [23], E_H=1 MeV and α =2.5 [24]. The equilibrium (EQ) spectrum was added to the preequilibrium (PEQ) one. The level density parameters a in EQ spectra have been extracted from the fit to the neutron spectra in the region above the second neutron emission threshold. Pairing corrections for EQ calculations have been taken from [25]. We have assumed $\lambda_+ = CA^{-3}E^{-1}\omega_f(n,E)$ [13] and the constants C have been obtained from the fit to the high energy part of

neutron spectra.

The comparisons between the experimental and the theoretical neutron spectra for ^{55}Mn and ^{59}Co target nuclei are displayed in figs. 6 and 7. The full lines represent the sum of PEQ and EQ spectra. In PEQ calculations we have assumed that all nucleons in p3/2 and f7/2 subshells take part in the interaction with the incident neutron with the same probability. Dashed lines represent the calculations wich are equivalent to the usual Exciton model (UEM): E_H=20 MeV, n_π =Z and n_ν =N. The dotted lines in fig. 6 represent the PEQ contributions in corresponding calculations. We see that PEQ spectrum calculated with our model is shifted - with respect to UEM - towards the higher energy and the same holds for the proton spectrum. Since no proton spectra are available for these reactions we will not discuss them further. We note only that our model is not in contradiction with the experiment.

In figs. 8 and 9 the theoretical and the experimental nucleon spectra for the reactions ν + ^{51}V are given. In order to describe simultaneously (i.E. with the same C in λ_+) we had to assume that the unpaired proton in ^{51}V is preferentially excited and therefore n_π = 1 and n_ν = 8. The full lines represent our model while the dashed ones the UEM. It is clear that our model describes better both nucleon spectra. The bump in the proton spectrum which corresponds to the transition to the ground state can not be described with our simple model. The theoretical activation cross section $\sigma_{np}^{act,th}$ is-in our model- 21.5 mb. To this value the area of the bump ($\sim$ 4 mb) should be added which gives $\sim$25.5 mb while the recommended value [26]

is 33 ± 3 mb. If the last figure is correct than the γ-competition near the threshold of the second proton is not negligible. On the other hand $\sigma_{np}^{act,th}$ = 31 mb for UEM which is in good agreement with the recommended value. However the proton spectrum is not properly described.

The nucleon spectra from the reaction γ + ^{56}Fe are shown in figs. 10 and 11. The neutron spectrum was measured using natural iron samples. We have assumed that only ^{56}Fe isotope contributes to the observed spectrum. Since ^{56}Fe is even-even nucleus we have assumed n_π = 8 and n_ν =2 (full lines). One can see that our model is able to describe simultaneously both nucleon spectra better than UEM (dashed lines). For our model $\sigma_{np}^{act,th}$= 108 bm which is in good agreement with the recommended value 114 ± 10 mb [26]. The UEM gives 91.5 mb.

In figs. 12 and 13 the nucleon spectra from γ + ^{93}Nb reaction are given. Again in order to describe simultaneously both spectra we had to assume that g9/2 proton is preferentially excited and therefore n_π= 1 and n_ν=2 (full lines). If we assume that protons from g9/2 and p1/2 subshells are equally probably excited (i.e. n_π =3) we obtain the spectrum represented by the dashed-dotted line (fig. 13) which evidently overestimates the experiment. The quality of the fit to the neutron spectrum remains the same as for n_π =1 only the constant C changes due to $a_x(n)$ in eq. (7). The dashed lines again represent the UEM calculations.

To conclude this part of our report we would like to note that our model is able to quite successfully describe simultaneously the nucleon spectra. Further, our calculations seem to

support the existence of the odd-even effect as observed e.g. in [27]. In all our calculations presented the value of $\lambda_+(2,1)$ is close to $1.5.10^{22}$ s^{-1} which implies the widths of the states involved to be several MeV. This value is in sharp contradiction with the characteristic value (several hundreds of keV) of the multi-step compound reaction theory [28] with which the EM formally coincides. The question why remains open.

L i t e r a t u r e

[1] WRENDA 81/82, INDC(SEC) - 78/URSF, IAEA, Vienna, 1981

[2] J. Csikai, Nuclear theory for applications - 1980, IAEA--SMR-68/I, Vienna 1981, p. 215

[3] K. Debertin and U. Schötzig, Nucl. Meth. 158 (1979) 471

[4] Š. Gmuca and I. Ribanský, to be published in Nucl. Instr. Meth.

[5] V. Hnatowicz, Nucl. Instr. Meth. 161 (1979) 151

[6] Š. Gmuca and I. Ribanský, to be published

[7] G. W. Phillips and K. W. Marlow, Nucl. Instr. Meth. 137 (1976) 525

[8] Š. Gmuca and I. Ribanský, to be published in Acta Phys. Slovaca

[9] W. W. Bowman and MacMurdo, Atomic Data and Nuclear Data Tables 13 (1974)

[10] Tables of Isotopes, ed. C. M. Lederer and V. S. Shirley, 7-th ed., John Wiley and Sons, Inc., 1978

[11] U. Reus, W. Westmeier and I. Warnecke, GSI-Report 79-2, Darmstadt 1979

[12] D. Seeliger, Nuclear theory for applications, IAEA-SMR-43, Vienna 1980, p. 283

[13] E. Gadioli, Nuclear Theory for applications, IAEA-SMR-68/I

[14] J. J. Griffin, Phys. Rev. Lett. 17 (1966) 478

[15] H. Feshbach, A. Kerman and S. Koonin, Annals of Phys. 125 (1980) 429

[16] W. A. Friedman, M. S. Hussein, K. W. Mc Voy and P. A. Mello, Preprint IFUSP/P-258, Instituto di Fisica, Universidade de Sao Paulo, 1981

[17] I. Ribanský and Š. Gmuca, Neutron Induced Reactions, ed. I. Ribanský and E. Běták, Veda, Bratislava 1980; I. Ribanský, Fizika 11 (1979) Supplement 2, p. 39

[18] Š. Gmuca and I. Ribanský, Neutron Induced Reactions, ed. I. Ribanský and E. Běták, Veda, Bratislava 1980

[19] J. Dobeš and E. Běták, Nucl. Phys. A272 (1976) 353

[20] K. Bleuler and M. Beiner, Nuovo Cim. B52 (1967) 149

[21] D. Hermsdorf et al., Report ZfK-277 (U), 1977

[22] S. M. Grimes and R. C. Haight, Phys. Rev. C 19(1979) 2127; S. M. Grimes, R. C. Haight and J. D. Anderson, Phys. Rev. C 17 (1978) 508

[23] G. S. Mani, M. A. Melkanoff and I. Iori, Rapport C.E.A. 2379 and 2380, 1963

[24] K. Kikuchi and M. Kawai, Nuclear Matter and Nuclear Reactions, North-Holland, Amsterdam 1968

[25] P.E. Nemirovsky and Yu. V. Adamchuk, Nucl. Phys. 93 (1962) 551

[26] V. M. Bychkov et. al, INDC (CCP)-146/LJ, IAEA, Vienna 1980

[27] A. Chevarier et al., Phys. Rev. C 8 (1973) 2155

[28] S. Koonin, Course on Advances in Nuclear Theory and Nuclear Data for Reactor Applications, Trieste 1982, to be published

Figure captions

Fig. 1 The efficiency curves of our Ge(Li) detector: 1 = $\varepsilon_{FEP,F}$, 2 = $\varepsilon_{FEP,C}$, 3 = $\varepsilon_{TOT,F}$, 4 = $\varepsilon_{TOT,C}$.

Fig. 2 The transformation curve for ε_{FEP}.

Fig. 3 The transformation curve for ε_{TOT}.

Fig. 4 GWENN fit of a part of Eu γ-ray spectrum.

Fig. 5 The block scheme of our activation experiment.

Fig. 6 The comparison between experimental and theoretical neutron spectra for ν + ^{55}Mn reaction at 14 MeV. The full line represents calculations with our model and the dashed line the UEM calculations. The dotted lines represent corresponding PEQ contributions.

Fig. 7 The same as in fig. 6 for ν + ^{59}Co reaction.

Fig. 8 The same as in fig. 6 for ν + ^{51}V reaction.

Fig. 9 The comparison between experimental and theoretical proton spectra. The full and dashed-dotted lines represent calculations with our model and the dashed line the UEM calculations (for details see text).

Fig.10 The same as in fig. 6 for ν + ^{56}Fe reaction.

Fig.11 The same as in fig. 9 for ν + ^{56}Fe reaction.

Fig.12 The same as in fig. 6 for ν + ^{93}Nb reaction.

Fig.13 The same as in fig. 9 for ν + ^{93}Nb reaction.

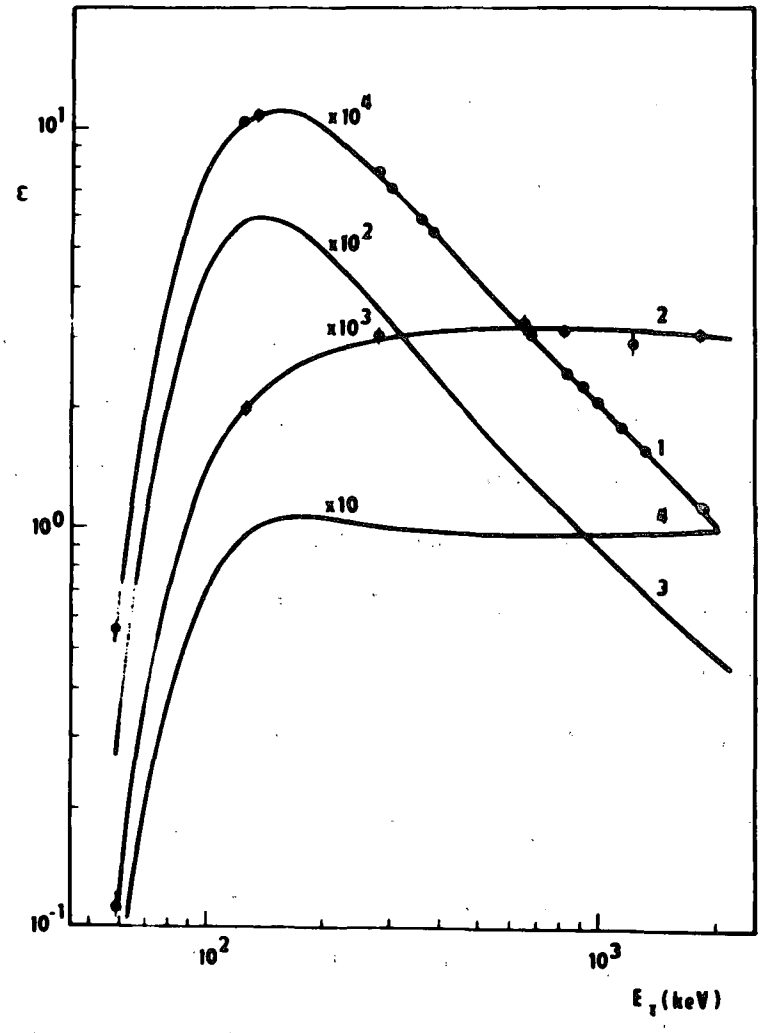

Fig. 1

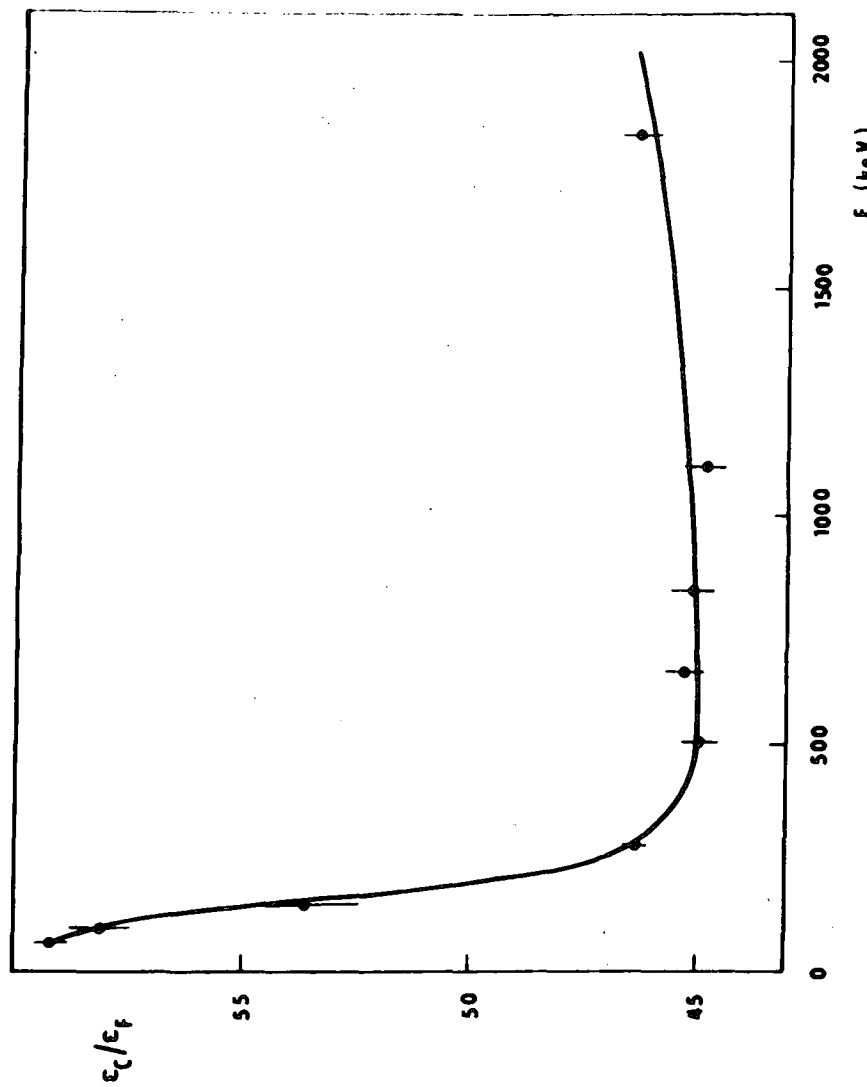
$\varepsilon_c/\varepsilon_f$
55
50
45
0
500
1000
1500
2000
ε_f(keV)

Fig. 2

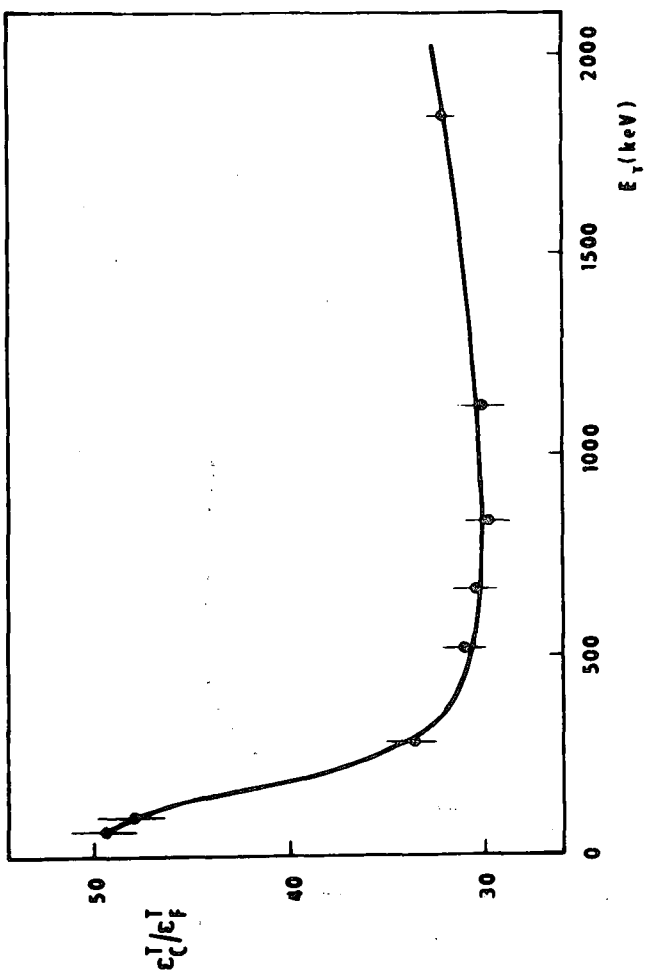
50
40
30
$\varepsilon_c^I/\varepsilon_F^I$
0
500
1000
1500
2000
E_γ(keV)

Fig. 3

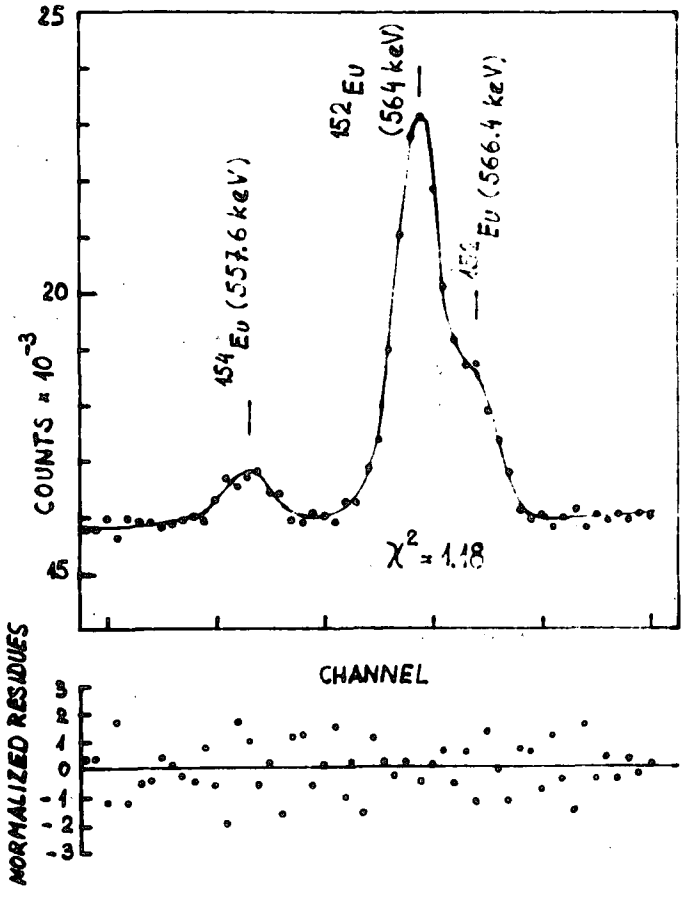
25
20
15
COUNTS x 10^-3
154 Eu (551.6 keV)
152 Eu (564 keV)
152 Eu (566.4 keV)
χ² = 1.18
CHANNEL
NORMALIZED RESIDUES
3
2
1
0
-1
-2
-3

Fig. 4

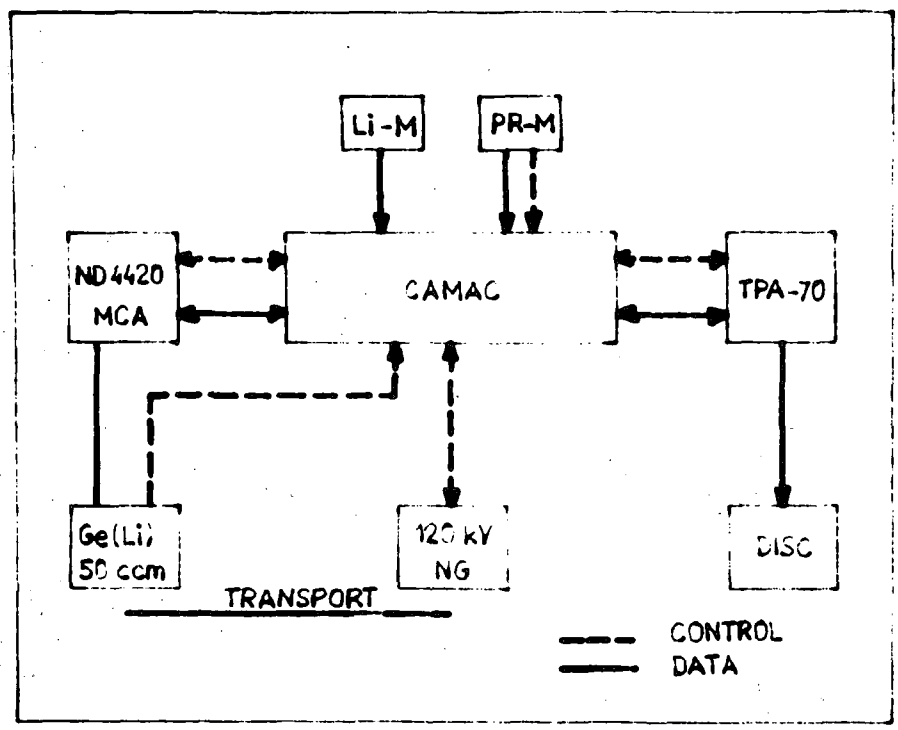
Li-M
PR-M
ND 4420
MCA
CAMAC
TPA-70
Ge(Li)
50 ccm
120 kV
NG
DISC
TRANSPORT
CONTROL
DATA

Fig. 5

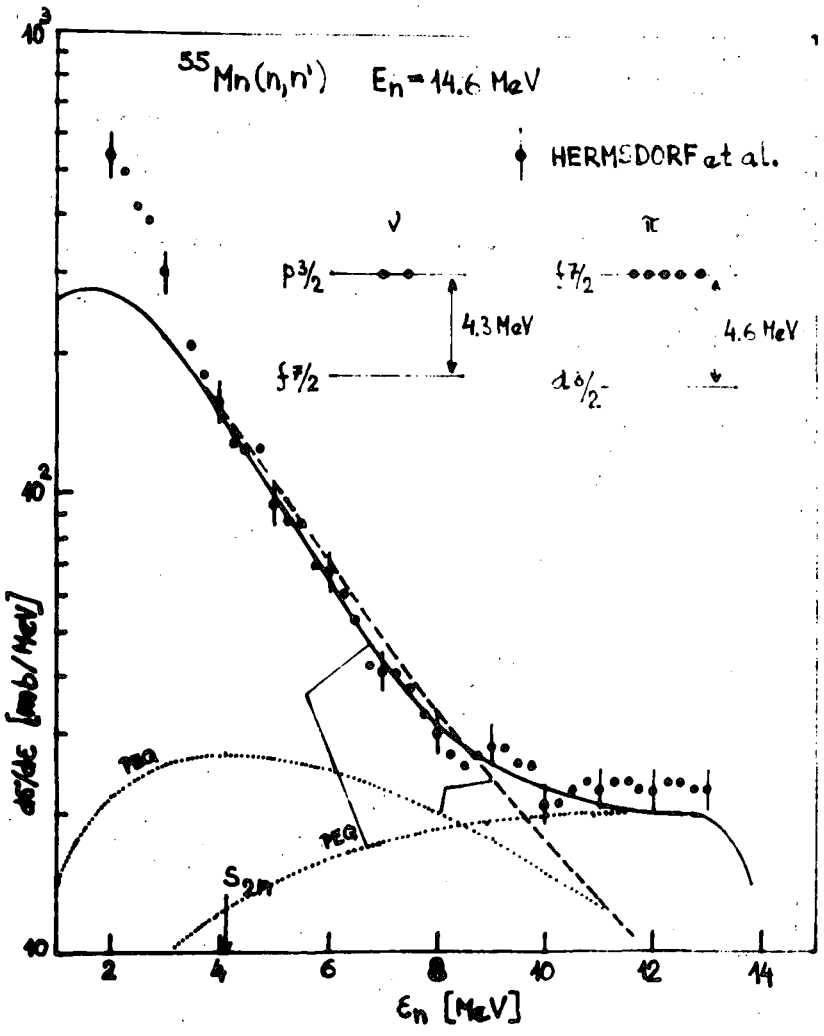
^{55}Mn(n,n') E_n = 14.6 MeV
HERMSDORF et al.
ν
π
$p_{3/2}$
$f_{7/2}$
4.3 MeV
4.6 MeV
$f_{7/2}$
$d_{5/2}$
PEQ
PEG
PEG
S_{2n}
10^3
10^2
10
2
4
6
8
10
12
14
dσ/dε [mb/MeV]
ε_n [MeV]

Fig. 6

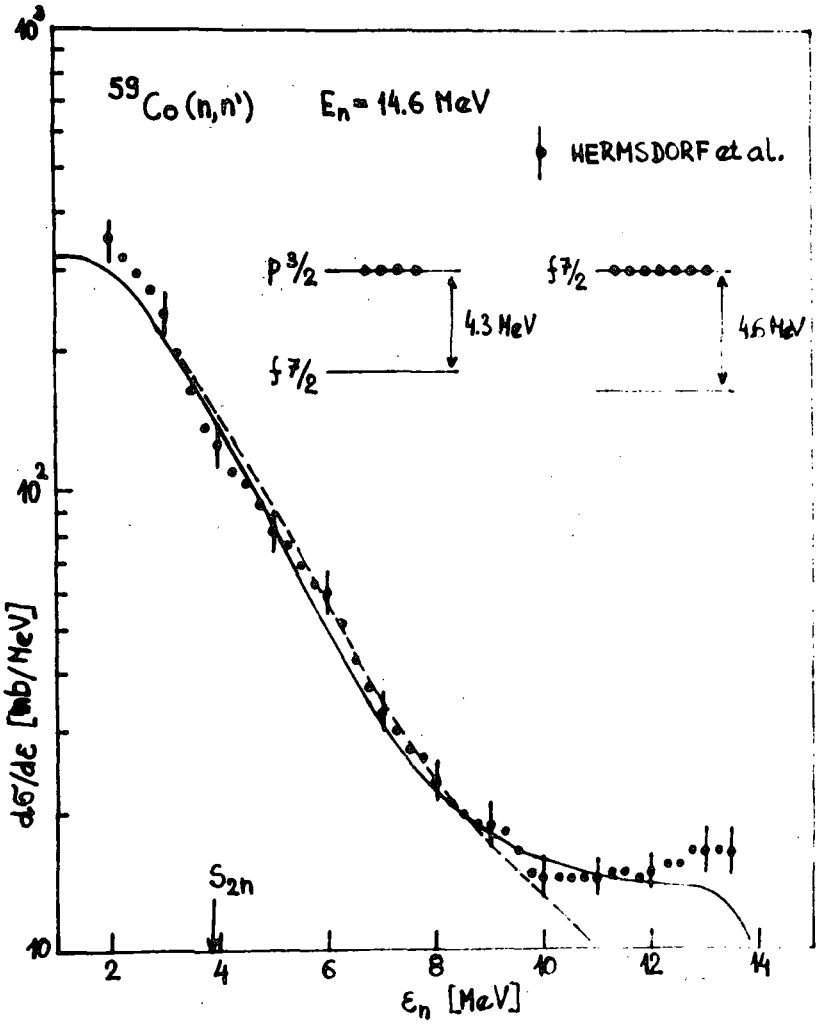
^{59}Co (n,n')
E_n = 14.6 MeV
HERMSDORF et al.
p 3/2
f 7/2
4.3 MeV
f 7/2
4.6 MeV
S_{2n}
dσ/dε [mb/MeV]
ε_n [MeV]

Fig. 7

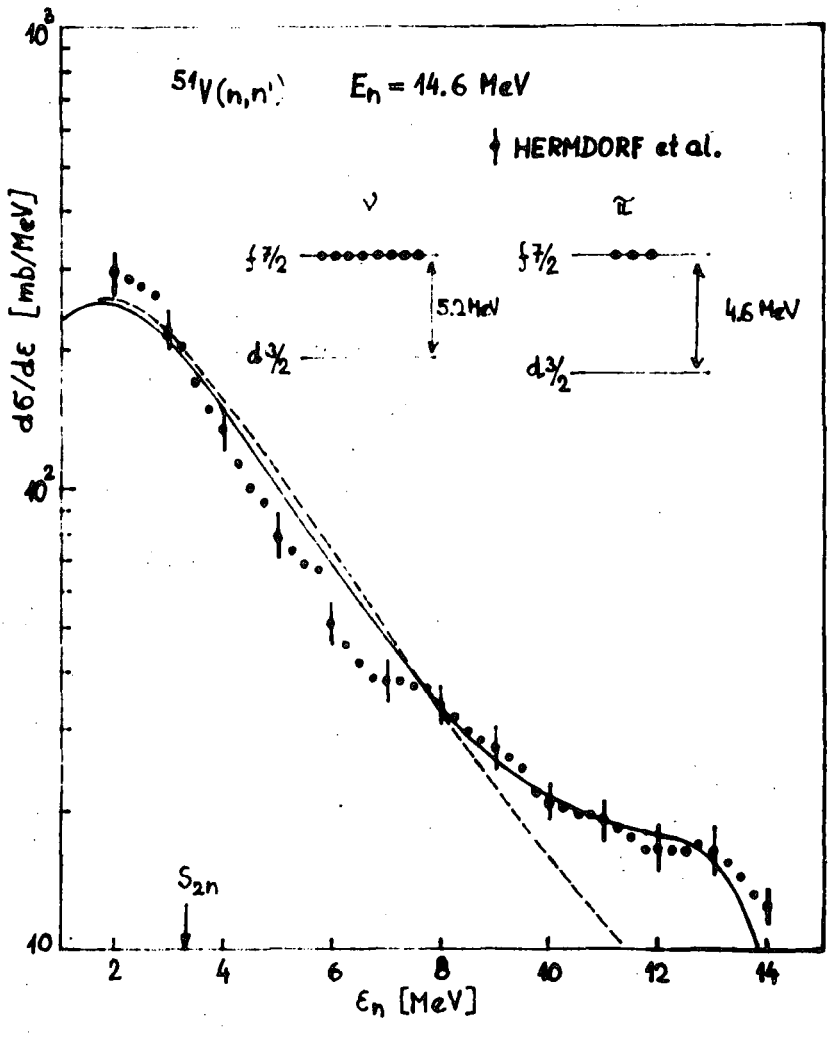
$^{51}V(n,n')$
$E_n = 14.6$ MeV
HERMDORF et al.
ν
π
$f_{7/2}$
$d_{3/2}$
5.2 MeV
4.6 MeV
S_{2n}
$d\sigma/d\varepsilon$ [mb/MeV]
ε_n [MeV]
10^3
10^2
10
2
4
6
8
10
12
14

Fig. 8

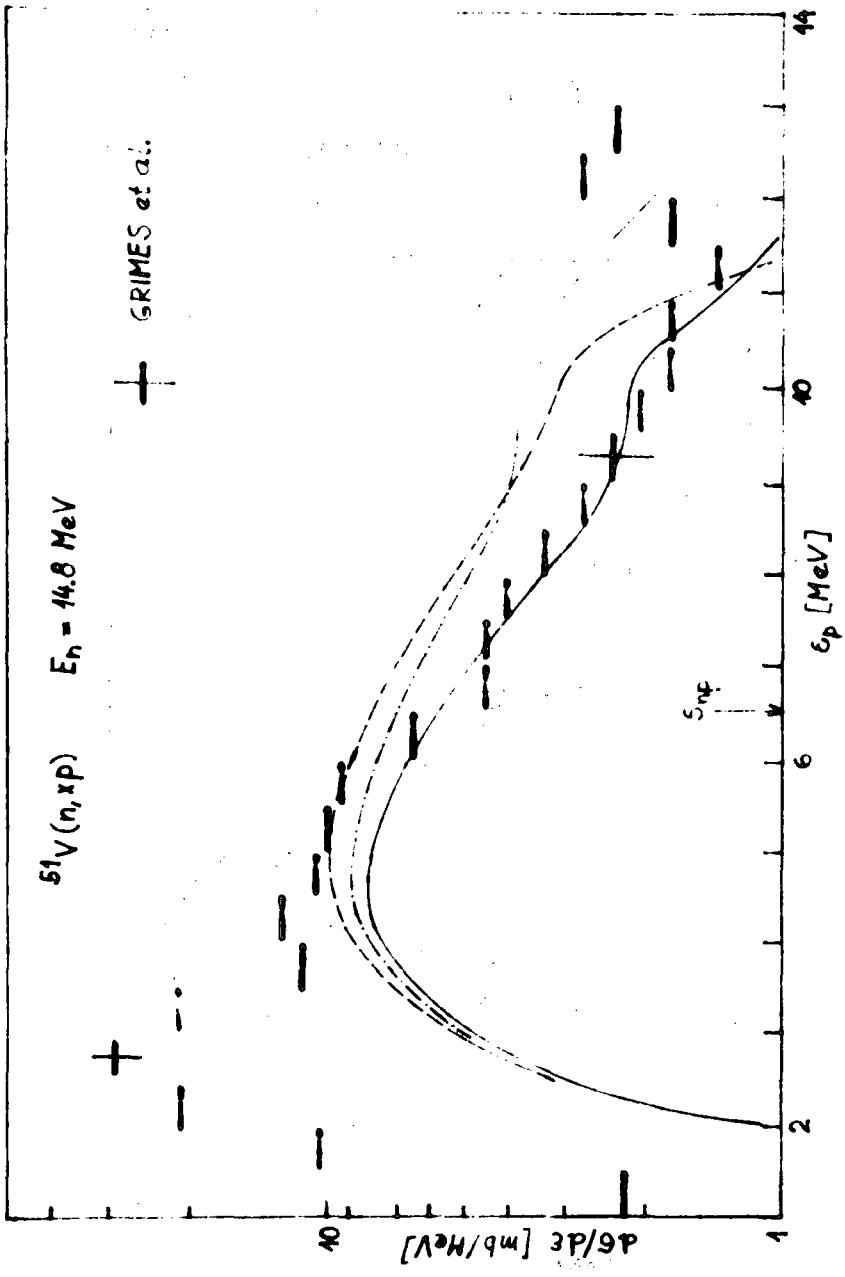
$51_V(n,xp)$ E_n = 14.8 MeV
GRIMES et al.
$d\sigma/d\varepsilon$ [mb/MeV]
ε_p [MeV]
ε_{max}
40
1
2
6
10
14

Fig. 9

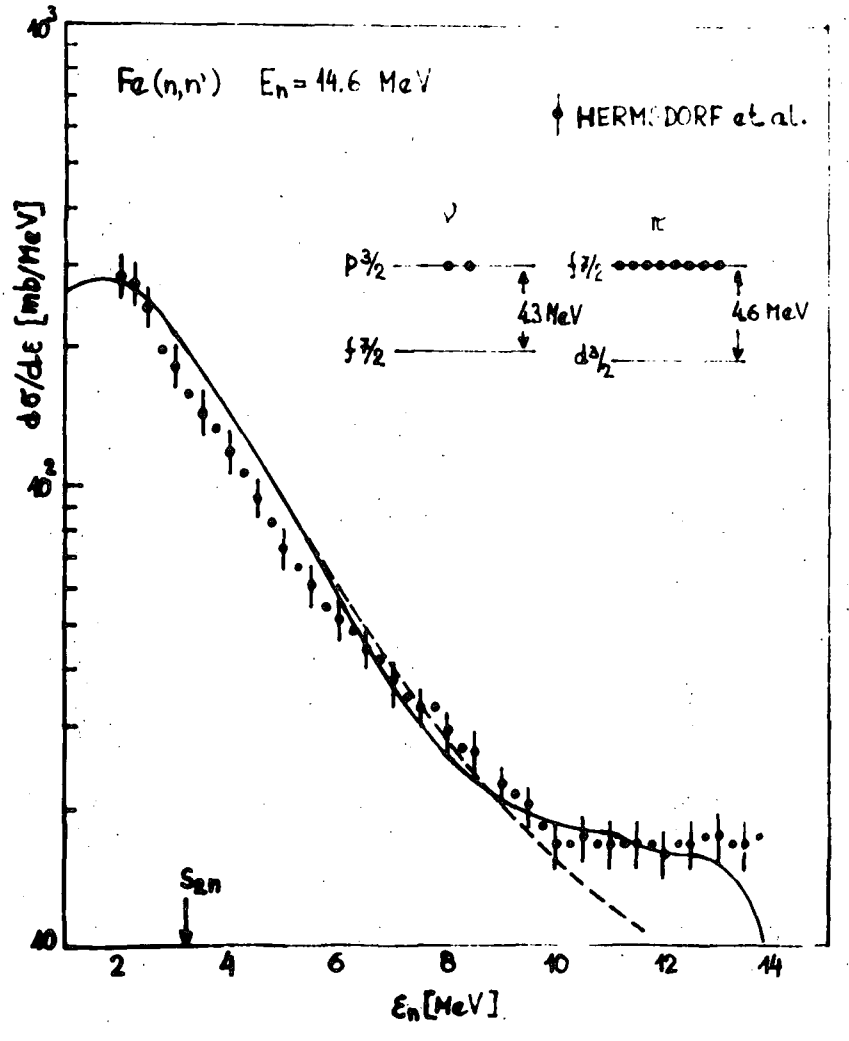
Fe(n,n') En = 14.6 MeV
HERMSDORF et al.
ν
π
p3/2
f7/2
4.3 MeV
4.6 MeV
f7/2
d3/2
Sen
dσ/dε [mb/MeV]
En [MeV]
2
4
6
8
10
12
14

Fig. 10

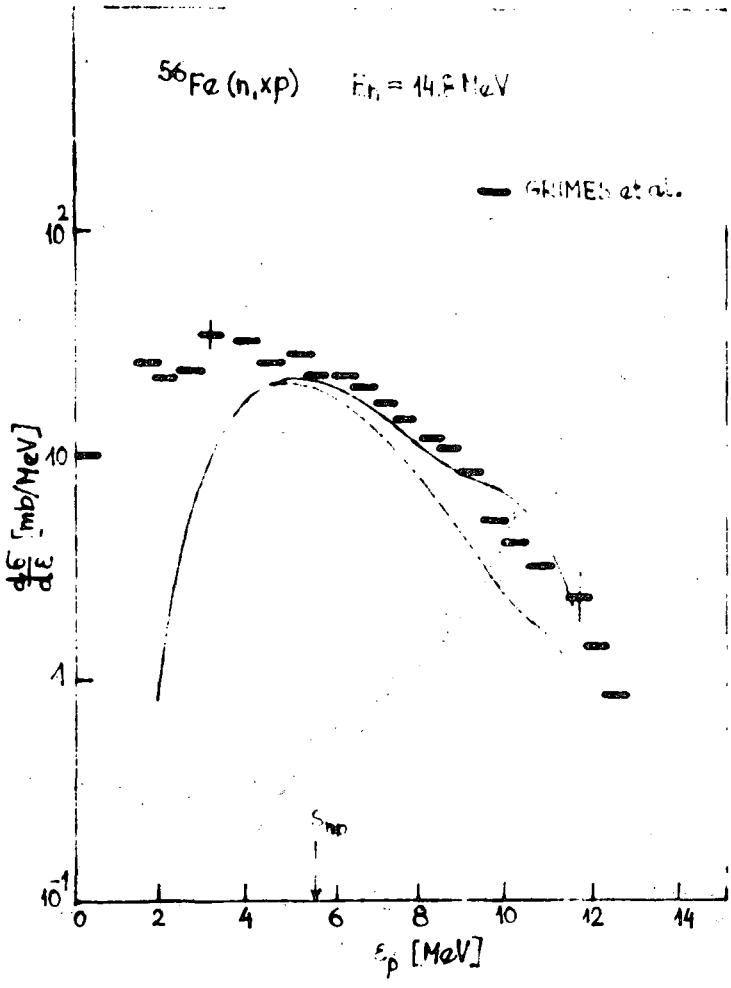
56Fe (n,xp)
GRIMES et al.
10^2
10
1
10^{-1}
$\frac{d\sigma}{d\varepsilon}$ [mb/MeV]
0
2
4
6
8
10
12
14
ε_p [MeV]

Fig. 11

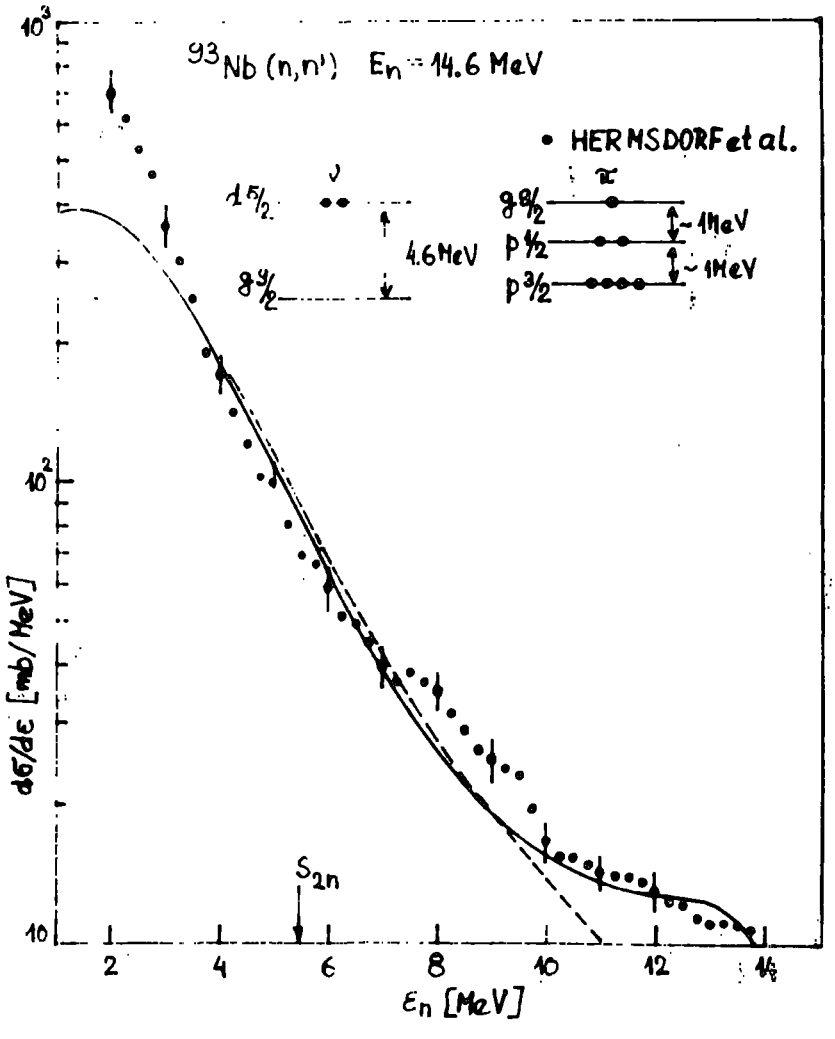
^{93}Nb (n,n') E_n = 14.6 MeV
• HERMSDORF et al.
ν
π
1f5/2
4.6MeV
g9/2
g9/2
~1MeV
p1/2
~1MeV
p3/2
dσ/dε [mb/MeV]
10^3
10^2
10
S_{2n}
2
4
6
8
10
12
E_n [MeV]

Fig. 12

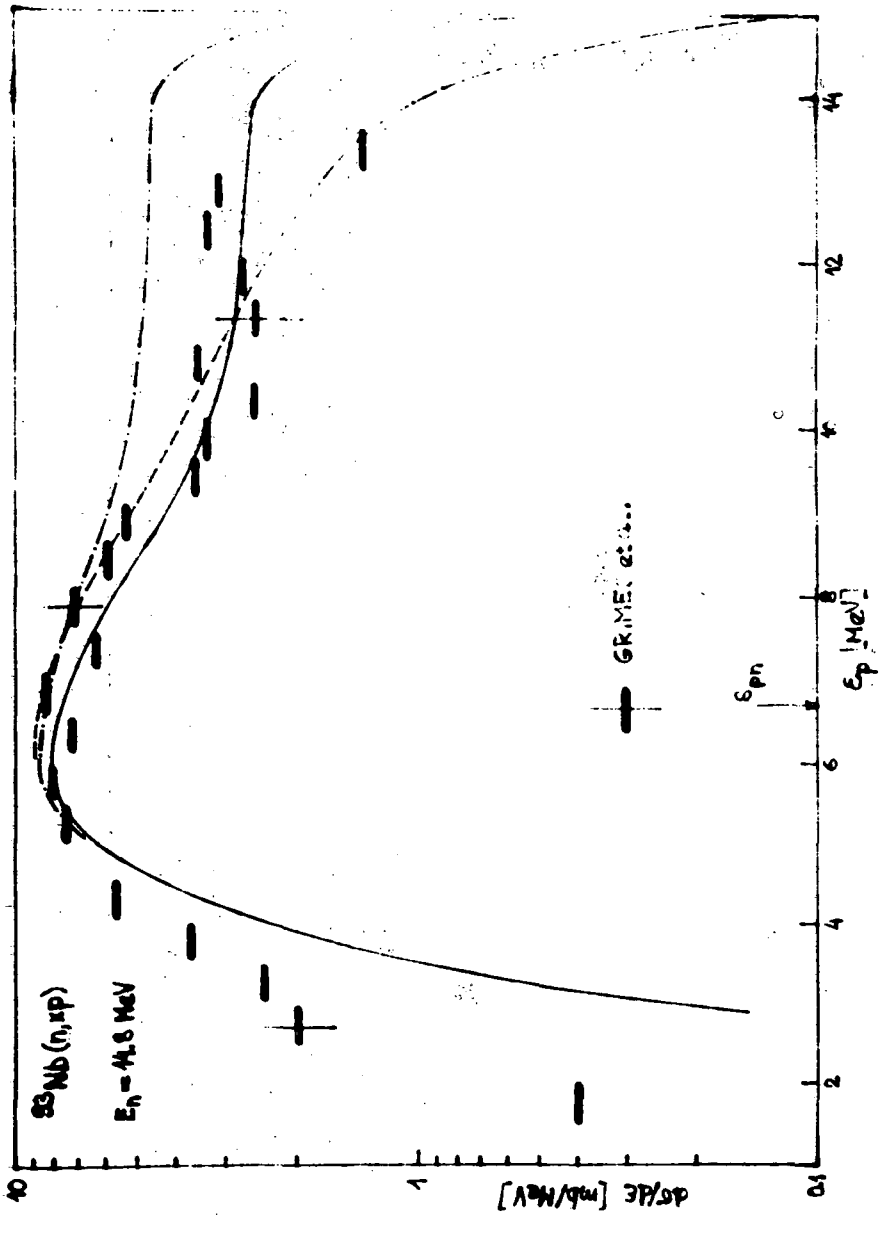
93Nb(n,xp)
En = 14.8 MeV
GRIMES et al.
Spn
Ep [MeV]
dσ/dE [mb/MeV]
10
1
0.1
2
4
6
8
10
12
14

Fig. 13